J. Water Environ. Nanotechnol., 4(1): 1-16 Winter 2019

ORIGINAL RESEARCH PAPER

The effect of polyethylene glycol grafted nanodiamond on antifouling properties of cellulose acetate membrane for Removal of BSA from Contaminated Water

Mahdi Seyfollahi[1, 2], Habib Etemadi[3],*, Reza Yegani[1, 2], Mahyar Rabiee[1, 2], Elham Shokri[3]

[1] Faculty of Chemical Engineering, Sahand University of Technology, Tabriz, Iran
[2] Membrane Technology Research Center, Sahand University of Technology, Tabriz, Iran
[3] Department of Chemical Engineering, University of Bonab, Bonab, Iran

Received: 2018-11-24 Accepted: 2018-12-30 Published: 2019-02-01

ABSTRACT

In this study, membranes were prepared by pristine and polyethylene glycol (PEG)-grafted nanodiamond (ND) embedded in cellulose acetate (CA) as matrix polymer via non-solvent induced phase separation method. The antifouling properties of the membranes were studied during filtration of bovine serum albumin (BSA) solutions and the governing fouling mechanisms of the membranes were also investigated using the Hermia model. Fourier Transform Infrared Spectroscopy (FTIR) and Thermal gravimetric analysis (TGA) confirmed that ND was successfully functionalized by PEG. CA/ND-PEG nanocomposite membranes have higher hydrophilicity, porosity, water uptake, mechanical strength and a lower amount of adsorbed protein than pure CA and CA/ND membranes. Besides, the antifouling performance of the CA/ND-PEG (0.5 wt.%) nanocomposite membrane also witnessed considerable improvement, in comparison with that of pure CA and CA/ND (0.5 wt.%) membranes. The obtained results showed that the best fit to experimental data for all membranes (pure and nanocomposite membranes) corresponds to the cake layer formation model.

Keywords: *Antifouling; Cellulose Acetate; Nanocomposite Membrane; Nanodiamond; Polyethylene Glycol*

How to cite this article
Seyfollahi M, Etemadi H, Yegani R, Rabiee Y, Shokri E.. The effect of polyethylene glycol grafted nanodiamond on antifouling properties of cellulose acetate membrane for Removal of BSA from Contaminated Water. J. Water Environ. Nanotechnol., 2019; 4(1): 1-16. DOI: 10.22090/jwent.2019.01.001

INTRODUCTION

Membrane process is extensively applied in many sectors of manufacturing industries including water and wastewater treatment, oil-water separation, medicine, pharmacy and foodstuff [1, 2]. Recently, membrane processes have taken up added importance because of the high efficiency of separation, low energy consumption, space saving, less or no use of chemicals and no harmful by-product formation, and so on [3, 4].

Ultrafiltration (UF) is the most commonly used pressure-driven process that is usually applied for protein separation and purification [5, 6]. However, high rejection of protein at the UF membrane interface causes a rise in the concentration of protein at the membrane interface, and accordingly, the osmotic pressure difference created across the membrane interface led to reducing the effective pressure drop across the membrane. Furthermore, proteins can be deposited on the membrane surface and inside the pores of the membrane, resulting in membrane fouling [6-9].

Fouling is a complex physicochemical phenomenon which is the result of the accumulation of foulant on the surface and/or within the pores of the membrane [10]. This phenomenon reduces the system productivity and increases the operational cost [11, 12]. The protein fouling of UF membranes

* Corresponding Author Email: *h_etemadi@bonabu.ac.ir*

is attributed to the hydrophobic nature of UF membranes that promotes protein-membrane interactions, causing adhesion of protein onto the membrane surface and within membrane pores [7, 9]. Hence hydrophilic polymer membranes are less prone to fouling than hydrophobic ones due to reduced hydrophobic interaction between proteins and membrane material [7, 13].

Modification of the membranes is widely aimed to improve membrane antifouling properties [11, 14]. Among all, incorporation of inorganic nanoparticles (NPs) into the polymer matrix of membranes is intensively studied [15-18]. Organic-inorganic composite membranes improve mechanical, chemical, thermal and antibacterial properties and also cause flux decline [19-21].

Among several choices, the nanodiamond (ND) particle has gained serious attention [22]. Important properties such as easy functionalization, narrow size distribution, hydrophilicity [23-25], antibacterial activity [15, 26, 27], biocompatibility [28, 29], chemical stability [28], thermal stability [29], non-toxicity [28-30], superior hardness and mechanical properties, resistance to harsh environments [28] and ease of surface functionalization [29], it has been selected as a reinforcement filler in the fabrication of nanocomposite materials.

Despite the advantages described above, pristine ND usually forms micro-sized agglomerates [31]. The presence of carbon impurities among the ND particles and consequently agglomeration of ND lead to poor dispersibility and weak interfacial interactions with polymer matrix [31, 32]. To reduce aggregation of NDs and improve their performance, surface functionalization is widely employed. Among several hydrophilic additives, polyethylene glycol (PEG) is most commonly used to enhance the hydrophilicity of the membrane [33].

PEG is one of the most utilized additives for membrane fabrication due to its hydrophilicity, low toxicity, good biocompatibility and low cost [33, 34]. PEG molecules can migrate from membrane matrix to coagulation bath due to their solubility in water, which promotes the formation of fully developed macropores [35]. Thus PEG enhances pore formation, increases the porosity and pore size, improves pore interconnectivity and introduces hydrophylicity [36]. However, when PEG is grafted with another reagent, in an aqueous solution, the oxygen atoms in PEG form strong hydrogen bonding with water molecules and therefore the entropy and mobility of its surrounding water declines, preventing proteins and other biological molecules from approaching it. This phenomenon is considered as a steric stabilization effect [37, 38].

In our previous work, PEG-grafted NDs was used in order to improvement of antifouling properties of the CA membrane for removal of HA from contaminated water [41]. The obtained results from that work showed that nanocomposite CA membrane containing 0.5 wt.% PEGylated ND exposes high hydrophilicity, high porosity, low HA adsorption capacity, high abrasion resistance and excellent antifouling properties due to the strong hydrogen bonding of water molecule to the oxygen atoms in PEG molecules, which prevents HA from approaching the surface. However, the structures and average molecular weight of BSA and HA are different from each other. Also according to our knowledge, there is no report about embedded PEG-grafted NPs in CA membrane in order to BSA separation.

In the current study, PEG-grafted NDs were employed to fabricate ND embedded cellulose acetate (CA) nanocomposite membrane via non-solvent induced phase separation (NIPS) method. This study focuses on the incorporation of pristine ND, PEG grafted NDs (ND-graft-PEG) in CA for investigating the impact of NPs on the performance and fouling behavior of CA membranes in protein purification. CA is suitable and is commonly used the material in preparation of UF membranes [3, 39]. Advantages of CA over other polymers are moderate flux, moderate salt rejection, highly non-toxic, high biocompatibility, good film-forming properties and excellent hydrophilicity, which help enhance the anti-fouling property [22, 40, 41]. However, the application of CA in UF membrane preparation is limited because of such drawbacks as poor chemical resistance and poor mechanical strength. Therefore it can be used only in the narrow temperature range, and high biodegradability, thereby reducing membrane lifetime and usage. Hence the modification of CA membranes takes up added importance [7, 39].

The effects of NPs on the performance, morphology, mechanical resistance, hydrophilicity, and the fouling behavior of CA membranes during the filtration of BSA protein were investigated. The fouling mechanisms of the fabricated membranes were analyzed using Hermia (classic) model.

EXPERIMENTAL

Materials

Cellulose acetate (M_n=30000) was purchased from the Sigma-Aldrich. Nanodiamond (ND) with individual sizes ranging from 4 to 6 nm was purchased from Sigma-Aldrich. Polyethylene glycol (PEG) with an average molecular weight of 200 (PEG 200) as the hydrophilic modifier was obtained from Sigma-Aldrich. Thionyl chloride ($SOCl_2$), triethylamine and N,N-dimethylformamide (DMF) for modifying ND were purchased from Merck. BSA was purchased from Sigma-Aldrich to study the fouling behavior of the membranes. All the chemicals were used without further purification.

ND functionalization

We used "grafting to" method in order to functionalize ND with PEG, as was reported in the literature [42]. In this method, the ND surface was firstly oxidized in order to create carboxyl groups and then reacted with thionyl chloride to convert the carboxylic acids to acyl chlorides. The acyl chloride groups were subsequently reacted with PEG in the presence of triethylamine to generate PEG conjugated ND, denoted by ND - PEG.

Air oxidation of ND

ND was placed in 430 °C for 1.5 h in the vicinity of air in order to oxidize hydroxyl groups on the ND surface to carboxyl groups [31]. This method is inexpensive, environmentally friendly, scalable, and selective for the removal of carbon impurities. Furthermore, it becomes hydrophilic with respect to chemically oxidation method.

Grafting PEG to ND

The method of grafting PEG to carboxylated ND was reported in the literature [43]. Firstly, 50.26 mg carboxylated ND and 2 mL anhydrous dimethyl formamide (DMF) were sonicated in a water bath for 30 min. The mixture was added to 20 mL thionyl chloride ($SOCl_2$) and refluxed at 70 °C for 24 h to convert the carboxyl groups to acyl chloride groups (ND – COCl). The mixture was evaporated with a rotary evaporator to remove excess $SOCl_2$ at 40 °C. After adding 20 mL anhydrous DMF, 50.48 mg PEG and 2 mL triethylamine, the mixture was refluxed for 24 h at 90 °C, separated by centrifugation and washed with methanol and distilled water for five times, respectively, to remove excess PEG, and ND-PEG was thus obtained.

Preparation of membranes

CA/ND-PEG flat sheet nanocomposite membranes were prepared by the phase inversion, induced by immersion precipitation technique [2, 39, 44]. Different concentrations of ND-PEG ranging from 0 to 0.75 wt% (the weight percentage of ND-PEG based on total polymer weight) were added to CA. The concentration of DMF was maintained at a constant level of 82.5 wt% of the total casting solution in each case.

The rest of the NPs were added to DMF and stirred (Shimi Fan Company, Iran) for 4 h at room temperature. The mixture was sonicated (WOSON Company, China) at 50 kHz for 3 h to ensure the homogeneous spread of the NPs and break up the agglomerates. Then CA (17.5 wt.%, by weight of the solution) was added to the initial mixture and dissolved in the solvent at 2000 rpm for 15 h.

The casting solutions were then degassed at room temperature for 24 h to complete the removal of any air bubbles. Then, the casting solutions were cast onto a glass plate using a thin film applicator by adjusting the thickness of 200 μm. The cast films were subsequently immersed in a distilled water bath as non-solvent for the leaching out of the solvent from the membrane surface.

Characterization

FTIR analysis

In order to identify the quality of created functional groups on the samples, Fourier Transform Infrared Spectroscopy (FTIR) was studied by a VERTEX 70 FTIR spectrometer (Bruker, Germany) in the range of 4000–400 cm^{-1}. The sample pellet of NPs for the FTIR test was prepared by mixing the particles with KBr.

Thermal analysis

The thermal behavior of the sample was determined using a PerkinElmer Pyris Diamond TGA system at a heating rate of 10 °C /min from room temperature to 750°C.

Field Emission-Scanning Electron Microscope (FE-SEM) analysis

The surface and cross-section morphologies of the prepared membranes were examined by Field Emission-Scanning Electron Microscope (FE-SEM) (MIRA3 FEG-SEM, Tescan). Cross-section samples were frozen and fractured in liquid nitrogen. All samples were coated with gold by sputtering before observation in order to make them conductive.

Tensile test

A tensile test machine (STM-5, SANTAM) was used to evaluate the mechanical properties of the membranes. The samples were cut into 50 mm × 5 mm in length and width, respectively. The effective length was 30 mm and two 5 mm edges were stuck in the machine. Each membrane sample was stretched at an extension rate of 10 mm/min at room temperature. Three trials were conducted for each sample and the mean values were reported.

Static contact angle measurement

The hydrophilicity of membranes was evaluated by measuring the static surface contact angle of the membrane surface using a contact angle goniometer (PGX, Thwing-Albert Instrument Co.). The average of 5 measurements on different locations of samples was reported.

Water content

Water content tests were conducted to study the adsorption of water to CA-ND-PEG nanocomposite membranes. In this regard, different pieces of samples were soaked in water at room temperature for 24 h. Then the weight of the wetted membrane (W_{wet}) was measured after mopping it with filter paper. The wet membranes were placed in 50 °C for about 24 h and thereafter, the weight of dry membrane (W_{dry}) was determined. The water content was calculated by the following Eq. (1) [44]:

$$U\% = \left(\frac{W_{wet} - W_{dry}}{W_{dry}}\right) \times 100 \quad (1)$$

The average of 3 samples of each membrane was reported.

Membrane porosity

The porosity of different CA/ND-PEG nanocomposite membranes was evaluated using Eq. (2) [44]:

$$\varepsilon(\%) = \frac{(W_{wet} - W_{dry})/D_{water}}{(W_{wet} - W_{dry})/D_{water} + (W_{dry}/D_{polymer})} \times 100 \quad (2)$$

Where ε (%) is membrane porosity, W_{wet} is the wet sample weight (g), W_{dry} is the dry sample weight (g), D_{water} (0.997 g cm^{-3}) and $D_{polymer}$ (1.30 g cm^{-3}) are the density of water and polymer at 25 °C, respectively. The average of 3 samples of each membrane was reported.

Static protein adsorption experiments

BSA was used as a model protein to characterize the anti-fouling capabilities of the membranes. BSA solution (1 g/l) was prepared by dissolving BSA in phosphate buffer solution (PBS, pH 7.0). The membranes were cut into small pieces (1 cm ×1 cm) and immersed into 5 ml BSA solution for 24 h at room temperature to allow for adsorption equilibrium. After reaching the adsorption equilibrium, the membranes containing adsorbed proteins were removed from the basic solution. Finally, the amount of protein adsorbed on the membrane was calculated by a mass balance using initial and final concentrations of BSA solutions measured by UV spectrophotometer (Bio Quest CE2501) at the wavelength of 280 nm.

The reduction percent of adsorbed protein in nanocomposite membrane compared to that in pure CA membrane was calculated using the following equation (Eq. (3)) [20]:

$$\%\,\text{Reduction} = \left(\frac{A - B}{A}\right) \times 100 \quad (3)$$

Where A and B are the amounts of adsorbed protein (μg/cm^2) by pure and nanocomposite CA membrane, respectively.

Pure water flux measurement

Pure water flux tests were determined using a dead-end filtration system having 5 cm^2 of membrane area. After compaction, the experiment was carried out at 1.4 bar and permeate was collected for a certain time. The water flux was calculated using the following equation:

$$J_0 = \frac{V}{A \times \Delta t} \quad (4)$$

Where J_0 is pure water flux (L/m^2.h), V is the permeate volume (L), A is membrane surface area (m^2), and Δt is the permeation time (h).

Fouling analysis

Theory of fouling mechanisms

Hermia presented models to predict the mechanism of fouling, which is responsible for flux decline under constant filtration pressure. These models for power-law non-Newtonian fluids can be written in a common mathematical form [13, 45]:

$$\frac{d^2t}{dV^2} = k\left(\frac{dt}{dV}\right)^m \quad (5)$$

Where V is the filtrate volume of filtration, t the

time of operation, k is the resistance coefficient and m is a constant kinetics parameter which characterizes the fouling model. For each value of m, a fouling mechanism is described: m = 2 for complete blocking which means that each settled particle on membrane surface will seal off pore entrances and prevent flow, m = 3/2 for standard blocking (also termed as internal pore blocking) implies that small size solutes deposit or adsorb onto the pore walls in the membrane and constrict its radius, m = 1 for intermediate blocking which is similar to complete blocking but assumes that particles settle on each other and seal off some pores, m = 0 for cake filtration model and this indicates that for fouling occurs due to the formation of a layer of particles on the membrane surface [22, 46].

The permeate flux is expressed as:

$$J = \frac{1}{A}\frac{dV}{dt} \quad (6)$$

Using the flux expression (Eq. (6)), the flux decline expression can be written as [13, 45]:

$$\frac{dJ}{dt} = -kJ(AJ)^{2-m} \quad (7)$$

For each value of m (2, 1.5, 1 or 0), the analytical solutions of the models are summarized in Table 1.

Fouling experiments

The effects of pure and functionalized NPs on the BSA protein purification and the improvement of membrane fouling behavior were investigated. BSA protein solution was prepared by dissolving 1 g of BSA in 1 L of standard (0.1 M) phosphate buffer saline (PBS) solution at pH of 7.2. After measuring the pure water flux J_1, the membrane holder was connected to the protein dead-end filtration system and the system was pressurized. The permeate flux J_p, was measured for every 10 min throughout the 180 min of filtration at constant trans-membrane pressure (TMP) of 1.4 bar. After 180 min of protein filtration, the membrane was rinsed with distilled water and the cake layer formed on the membrane was gently removed mechanically by a sponge. Finally, the membrane was connected to the pure water filtration system and the pure water flux after rinsing was measured and labeled as J_2. Using J_P, J_1, and J_2, we can determine the fouling-resistance of the membranes and achieve useful information about the flux behavior.

The reversible fouling ratio (RFR), irreversible fouling ratio (IFR) and total fouling ratio (TFR) of the membrane were evaluated using the following equation [13, 33]:

$$RFR = \left(\frac{J_2 - J_p}{J_1}\right) \times 100 \quad (8)$$

$$IFR = \left(\frac{J_1 - J_2}{J_1}\right) \times 100 \quad (9)$$

$$TFR = \left(\frac{J_1 - J_p}{J_1}\right) \times 100 \quad (10)$$

Finally, in order to compare the antifouling properties of the membranes, flux recovery (FR) was evaluated using the following equation:

$$FR = \left(\frac{J_2}{J_1}\right) \times 100 \quad (11)$$

Membrane performance

The retention of BSA protein was investigated for the prepared membranes by measuring the concentration of the BSA in permeate by using a UV spectrophotometer (Bio Quest CE2501) at 280 nm (the concentration of BSA for samples was

Table 1. Four typical Hermia fouling models.

Fouling model	m	Flux expression	Linear form
Cake filtration	0	$J = \frac{J_0}{(1+J_0^2 kt)^{1/2}}$	$\frac{1}{J^2} = \frac{1}{J_0^2} + kt$
Intermediate blockage	1	$J = \frac{J_0}{1+J_0 kt}$	$\frac{1}{J} = \frac{1}{J_0} + kt$
Standard blockage	1.5	$J = \frac{J_0}{(1+J_0^{1/2} kt)^2}$	$\frac{1}{\sqrt{J}} = \frac{1}{\sqrt{J_0}} + kt$
Complete blockage	2	$J = J_0 \exp(-kt)$	$\ln(\frac{1}{J}) = \ln(\frac{1}{J_0}) + kt$

measured by standard curve) and the BSA rejection of the membrane was calculated by the following equation:

$$R(\%) = (1 - \frac{C_p}{C_f}) \times 100 \quad (12)$$

Where C_p and C_f are the concentrations of BSA protein in permeate and feed sides, respectively.

RESULTS AND DISCUSSION

ND-PEG characterization

FTIR analysis

In order to confirm the formation of desired functional groups on the ND, FTIR analysis was carried out. Fig. 1 shows the spectra for ND, ND-COOH, and ND-PEG. The FTIR spectrum of ND displays characteristic peaks of ND at 1177 cm^{-1} (C-O-C), 1764.8 cm^{-1} (C=O), 3486.2 cm^{-1} (-OH), 2856.8 and 2981.7 cm^{-1} (asymmetric and symmetric C–H stretching, respectively) [42]. In case of air oxidized ND; ND-COOH, the intensity of the hydroxyl absorption bond was obviously decreased while carbon-hydrogen absorption bonds disappeared, suggesting that these functional groups were oxidized to a carbonyl group. As observed in Fig. 1, the intensity of the carbonyl absorption bond was obviously enhanced and shifted from 1764.8 to 1798 cm^{-1}, indicating a structural change after the oxidization of ND.

For ND-COOH, C-H bands (vibration at 2981.7 and 2856.8 cm^{-1}) in pure ND disappeared completely and the absorption peak of C=O was shifted to 1798 cm^{-1} due to the conversion of some oxygen-containing groups like ketone, alcohol, and ester to the carboxylic group [47].

The characteristic peak of carbon-hydrogen stretching appears at 2849.7 cm^{-1} and 2921 cm^{-1}, corresponding to the $-CH_3$ in PEG. In addition, other characteristic peaks of PEG chain at 3298, 1701.2, 1655.8, 1479.3, 1259.4, 1136, 1095.5 and 825.5 cm^{-1} were all observed in ND-PEG, indicating that PEG was indeed grafted to the surface of ND (Fig. 1).

TGA analysis

Fig. 2 shows the TGA curves of ND, ND-COOH, and ND-PEG. As presented in Fig. 2, the ND's weight decreased as temperature increased. The weight loss percentage of the ND was about 2% until 520 °C and then the ND was decomposed. The weight lost of ND-COOH was about 4% until the temperature reached 520 °C, suggesting that more functional groups were introduced onto the surface of the ND after air oxidation. As expected, the weight loss of ND-PEG was obviously greater than that of pristine ND and ND-COOH (about

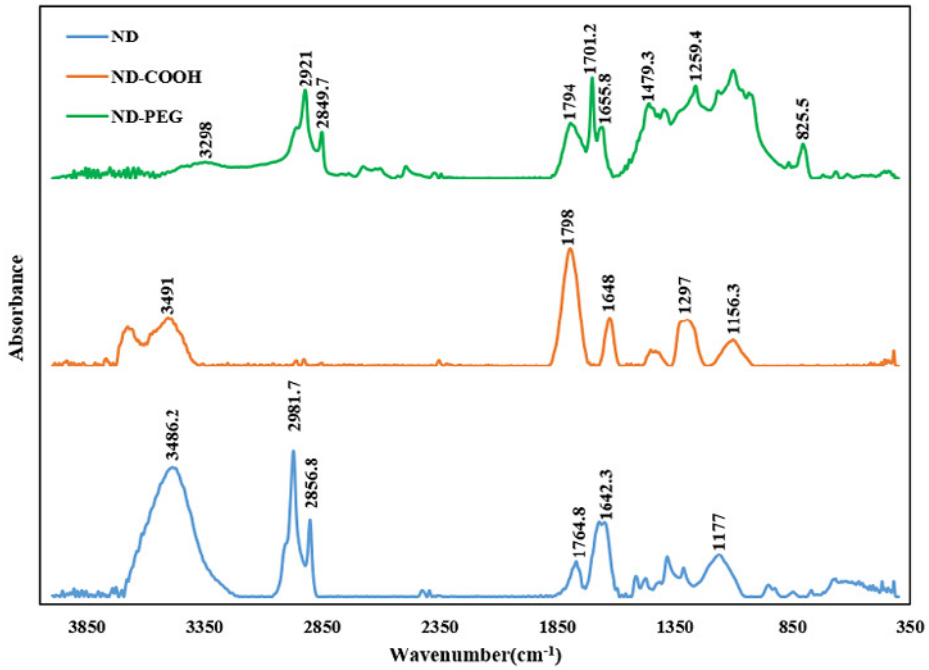

Fig. 1. The FT-IR spectra of pristine ND, ND-COOH and ND-PEG nanoparticles.

20%) due to the decomposition of the PEG chains bonded to the ND surface. These results demonstrated that PEG chain was conjugated to the surface of ND.

Membrane characterization

Membrane morphologies

The surface and cross-section morphologies of the selected membranes were studied by FE-SEM analysis. The influence of the addition of ND and ND-PEG on the membrane surface is shown in Fig. 3. It is obvious that in the absence of any ND, similar to other reports, the smooth membrane surface is formed on the top surface of pure CA membrane [44]. As depicted in Fig. 3b, when pure ND content is increased up to 0.5 wt%, the membrane porosity increases. This result may be considered as a consequence of acceleration of mass transfer rate between solvent and nonsolvent during phase inversion process due to the hydrophilic property of NDs, which would enhance interactions between components in the casting solution and coagulation bath. Also, as reported [48], mixing hydrophilic NPs to the matrix polymer could increase the amorphous nature of membranes and enhance the volume fraction among the polymer chains. Together with the fast exchange of solvent and non-solvent in the phase inversion process, the overall porosity of the prepared membranes was improved. Simultaneously immersing casting solution into the coagulation bath, casting solution is rapidly solidified at the interface between casting solution and non-solvent (water) because of the steep activity and concentration gradient of all components. Some fractured points are created when rapid solidification occurs. It is due to immitigable stresses produced by the shrinkage of the organic phase and pores formed after phase inversion is completed [49]. It is well documented that addition of hydrophilic ND to the casting solution could increase the coagulation rate during the phase inversion process by increasing the thermodynamic instability that induces more stresses in the solid polymer surface and results in

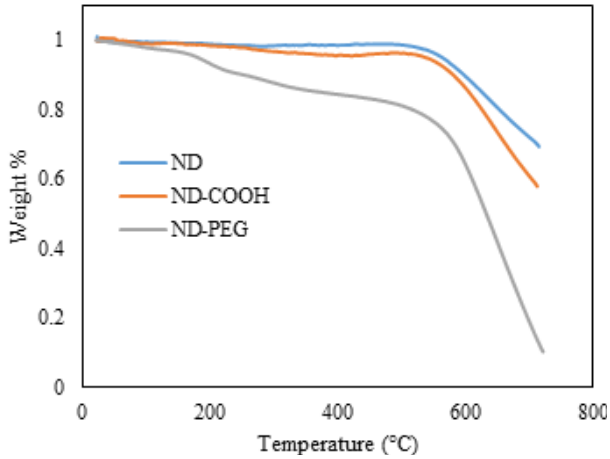

Fig. 2. TGA curves of pristine ND, ND-COOH and ND-PEG nanoparticles.

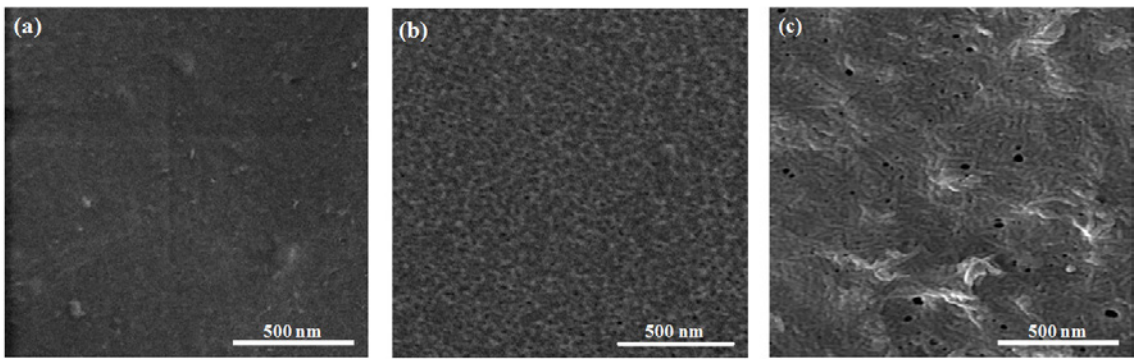

Fig. 3. Surface FE-SEM images of prepared membranes: (a) CA, (b) CA/ND (0.5 wt.%), (c) CA/ND-PEG (0.5 wt.%).

the formation of larger pores by fractured points [49]. Since ND-PEG is more hydrophilic than neat ND due to the presence of grafted PEG chain in ND-PEG surface, the increase in the surface pore size and porosity are more pronounced when CA/ND-PEG content increases up to 0.5 wt.% (see Fig. 3c).

The cross-section of the pure CA membrane, shown in Fig. 4a, demonstrated the asymmetric porous structure with both cellular pores and macrovoids. Macrovoids easily communicate with each other through the links provided by the sponge walls with a large number of micropores. The cross-sectional FE-SEM image of CA/ND (0.5 wt.%) nanocomposite membrane (Fig. 4b) demonstrated a great change in sub-layer morphology in the presence of ND particles in the dope solution. As mentioned earlier, the rate of solvent-nonsolvent exchange is accelerated with the addition of hydrophilic NDs. By adding pure

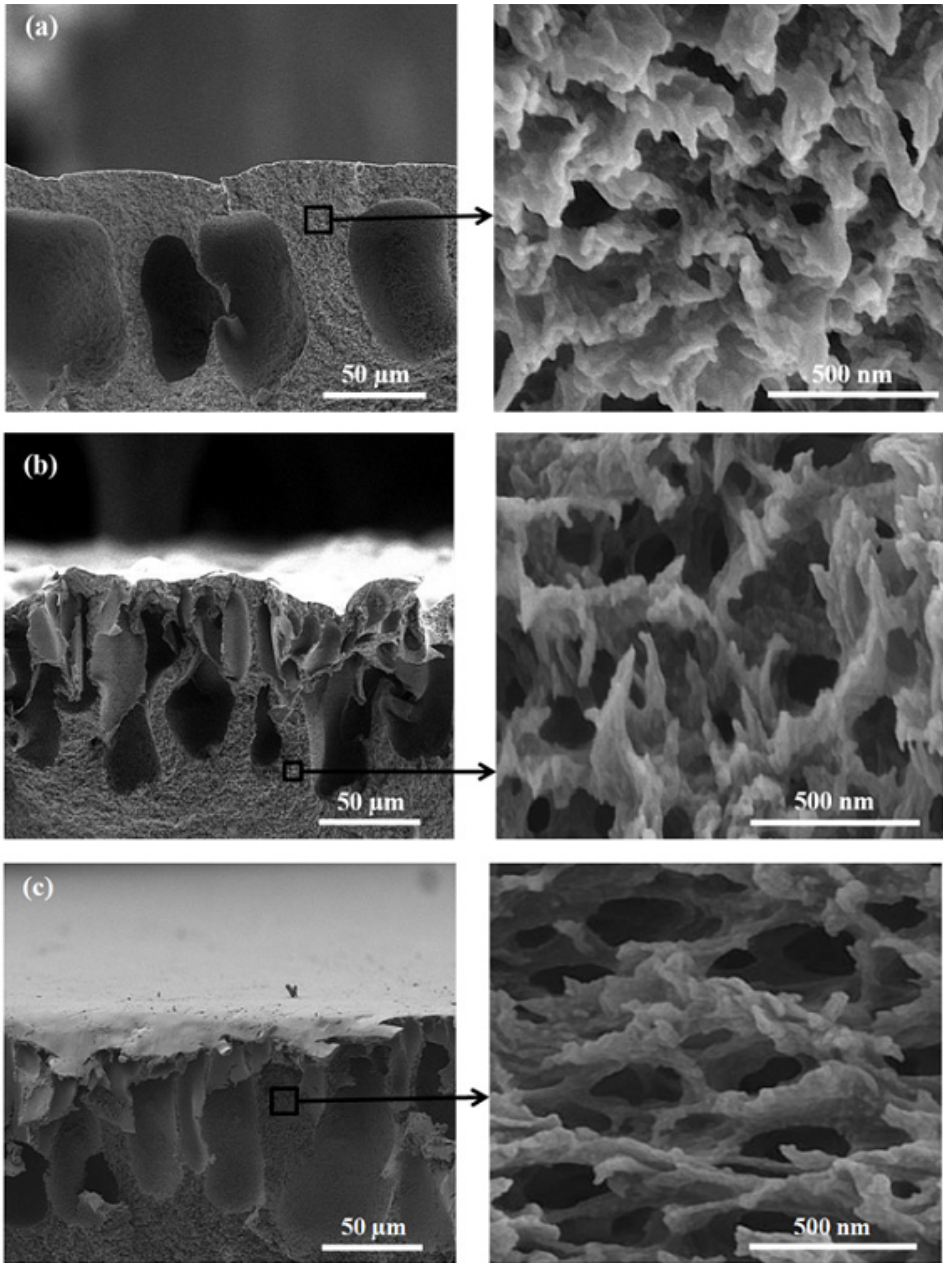

Fig. 4. Cross-section FE-SEM images of prepared membranes: (a) CA, (b) CA/ND (0.5 wt.%), (c) CA/ND-PEG (0.5 wt.%).

and functionalized ND particles, the number as well as the length of macrovoids increases, while the size of the macrovoids decreases. A severe increase in sponge walls was observed for the sample containing CA/ND (0.5 wt.%) and CA/ND-PEG (0.5 wt.%) NPs. It should be noted that the ND and ND-PEG are not discernible in the surface and cross-sectional FE-SEM images due to their small size (4-6 nm).

Mechanical strength

The testing results of mechanical properties are shown in Fig. 5. The obtained results show that the mechanical strength rises with an increase in the NPs' content up to 0.5 wt% of ND and ND-PEG and then declines with a further increase in the NPs' content (see Fig. 5a). It can be seen that the increase in the tensile strength of ND-PEG embedded CA membrane is more pronounced than pure ND embedded CA membrane. This could be due to the treatment of the ND surface, which reduces the tendency of the ND particles to join each other and form particle aggregates.

However, an excessive filler concentration may cause NPs aggregation and prevent them from dispersing uniformly in a polymeric matrix. That acts as a weak point and leads to decline in the mechanical stability of the fabricated membrane. Arthanareeswaran et al. [2] acquired similar observations for CA/SiO_2 blend UF membranes.

Fig. 5b reveals elongation at break of pure CA, CA/ND, and CA/ND-PEG nanocomposite membranes with various NPs. It can be seen that elongation at break of CA/ND-PEG (0.5 wt.%) membrane was larger than other samples due to the reinforcing effect of the ND-PEG particles and the presence of good interaction between NPs and CA matrix.

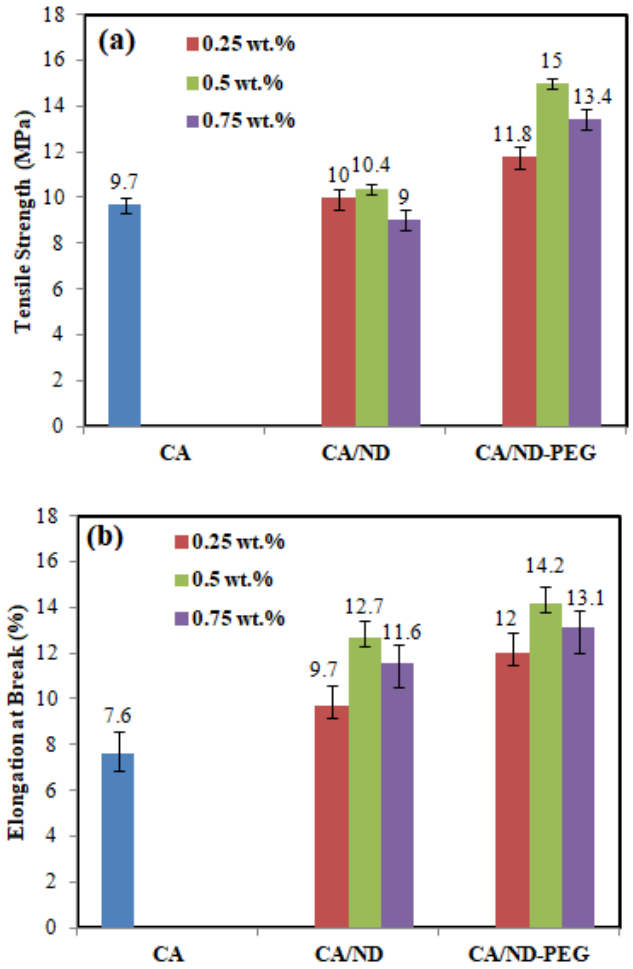

Fig. 5. Mechanical properties of pure and nanocomposite CA membranes; (a) tensile strength and (b) elongation at break.

Contact angle, porosity and water content

The membranes were characterized in terms of hydrophilicity, water content and effective porosity measurement. The results are summarized in Table 2. Surface hydrophilicity is the most important factor among membrane properties which could seriously affect the flux and antifouling ability of the membranes [50]. The hydrophilicity of the membrane surface can be evaluated by water contact angle measurement, as a lower contact angle reflects that the membrane surface is more hydrophilic. As presented in Table 2, it was found that the contact angle of the CA membranes decreased by adding ND due to the presence of a certain amount of hydrophilic groups on the NDs surface that made membrane more hydrophilic than pure CA. Furthermore, comparing the contact angle of nanocomposite membranes confirms that the CA/ND-PEG membrane is more hydrophilic than the CA/ND membrane due to the inherent hydrophilic characteristic of PEG attached to the ND surface. In addition to the surface functional groups, the surface porosity has a severely intense effect on the contact angle; with an increase in the surface porosity, the water drop could gradually penetrate into the pores due to the capillary force. That would decrease the contact angle.

In the case of both nanocomposite membranes, the contact angle decreases by increasing NPs and it reaches a minimum value when NPs concentration increase is 0.5 wt%. The reason is the increase in the hydrophilic functional group on the membrane surface. Any further increase in the NPs concentration would increase the contact angle, as observed in Table 2.

The trend in the variation of effective porosity is similar to water contact angle, as shown in Table 2. As we expect, modified membranes exhibited higher porosity than that of pure CA membrane, as discussed in membrane morphology section. By mixing the hydrophilic NPs with the casting solution, the volume fraction among the polymer chains as well as the rate of solvent and non-solvent exchange in the phase inversion process increased,

Table 2. Contact angle, porosity and water content of fabricated membranes.

Membrane	Water contact angles (°)	Water content (%)	ε (%)
CA	65.4	71.6	76.7
CA/ND (0.25 wt.%)	60.3	74.2	78.6
CA/ND (0.5 wt.%)	58	75	80.5
CA/ND (0.75 wt.%)	59.1	73.5	78.5
CA/ND-PEG (0.25 wt.%)	55.8	79.2	82.5
CA/ND-PEG (0.5 wt.%)	52.2	79.8	82.8
CA/ND-PEG (0.75 wt.%)	52.7	78.8	82.2

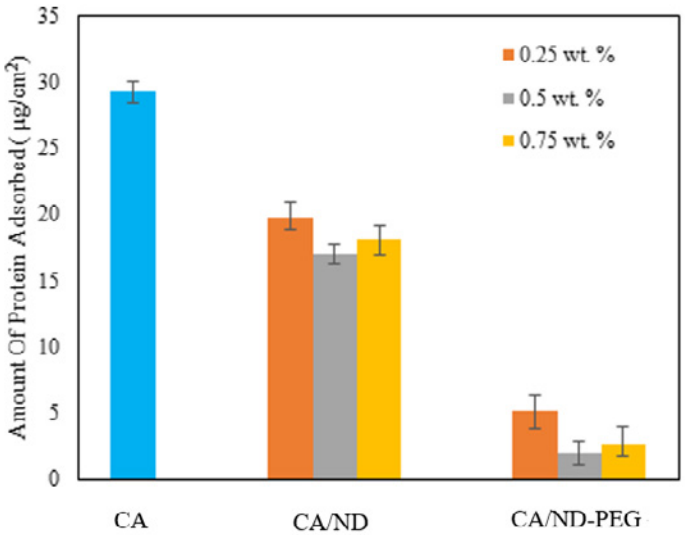

Fig. 6. Amounts of adsorbed protein via pure CA, CA/ND, CA/ND-PEG membranes.

increasing the membrane porosity. Moreover, the viscosity of the casting solution increases that reduces the rate of solvent and non-solvent exchange in the phase inversion process, which consequently reduced the membrane porosity [50-52].

The trend in membrane water content, shown in Table 2, was similar to both water contact angel and membrane porosity. The increase in the water content was also attributed to the increase of membrane hydrophilicity as well as surface porosity, which lead to an increase in the uptake of water through membrane pores. The obtained result showed good agreement with the findings reported by J. Dasgupta et al. [44].

Protein adsorption test

The amount of proteins adsorbed on the membrane is an important property that relates to its fouling-resistance ability according to which any decrease in protein adsorption is generally propounded as an important sign of anti-fouling property improvement. In this work, BSA is used to evaluate the protein repellency of prepared membranes. Fig. 6 and Table 3 show the amount and reduction percentage of adsorbed protein by fabricated membranes, respectively. In general, the protein repellent behavior is very similar to that of the water contact angle.

Table 3. Percent reduction of protein adsorption based on adsorbed proteins via pure CA membrane.

Membrane	Percent reduction of protein adsorption
CA/ND (0.25 wt.%)	32.42
CA/ND (0.5 wt.%)	41.98
CA/ND (0.75 wt.%)	38.23
CA/ND-PEG (0.25 wt.%)	82.59
CA/ND-PEG (0.5 wt.%)	93.52
CA/ND-PEG (0.75 wt.%)	91.13

Pure CA membrane shows the maximum protein adsorption about 29.3 μg/cm^2 and all of the nanocomposite membranes exhibited lower protein adsorption amount than the Pure CA membrane. It can be attributed to the enhanced hydrophilic property of the membrane surface, shown in Fig. 6. When the membrane hydrophilicity increases more water can be adsorbed to the surface of the membrane [53]. In other words, the free water fraction increases and subsequently enhances the protein repellent property [7]. The amounts of adsorbed protein were further decreased for the CA/ND-PEG nanocomposite membranes due to the improved antifouling behavior of PEG. PEG has excellent hydrophilicity, flexibility and unique coordination with surrounding water molecules in aqueous solutions that could bind a significant amount of water on the surface, leading to a sharp decrease in protein adsorption [54]. The protein adsorption amount decreased to 1.9 (μg/cm^2) for CA/ND-PEG (0.5 wt. %) nanocomposite membrane and the percent reduction of protein adsorption for this membrane was about 93.52 %. The results suggested that nanocomposite membranes containing ND-PEG have a better ability than pure CA membrane as well as CA/ND nanocomposite membrane to suppress protein adsorption.

Membrane performance

Pure water flux

The results of pure water flux of the pure and nanocomposite CA membranes with 0.5 wt.% NPs are illustrated in Fig. 7. The lowest value of pure

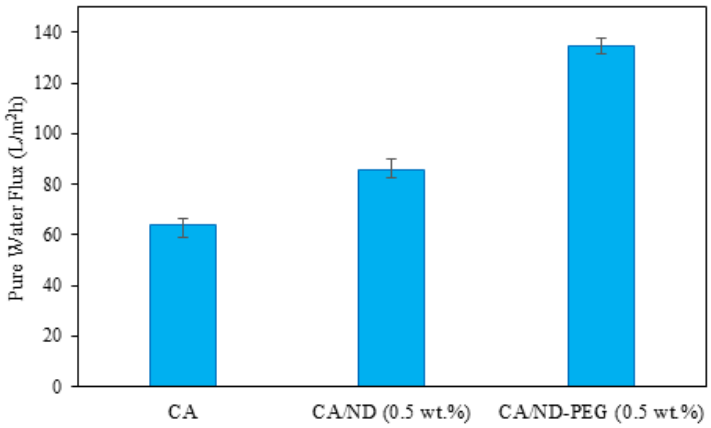

Fig. 7. Pure water flux of pure CA, CA/ND (0.5 wt.%), CA/ND-PEG (0.5 wt.%) membranes.

water flux 63.7 Lm^{-2} h^{-1} was obtained for pure CA membranes. The incorporation of ND and ND-PEG in CA membrane, increased the pure water flux value 85.75 and 134.75 Lm^{-2} h^{-1} for CA/ND (0.5 wt.%) and CA/ND-PEG (0.5 wt.%), respectively. This improvement in pure water flux may be due to the enhancement of porosity, surface pore size and hydrophilic property of the membrane. As shown in Fig. 3, the surface pore size of membranes increased by adding NPs to the casting solution. Grafting of PEG onto the ND was significantly effective in increasing the membrane surface hydrophilicity and enhanced the water permeability by attracting water molecules inside the nanocomposite membrane and facilitated their penetration through the membrane.

Membrane performance in BSA solution filtration

In order to investigate the antifouling behavior of the prepared membrane, filtration experiments were performed using BSA protein dissolved in aqueous solutions. Fig. 8 shows the flux decline during ultrafiltration of BSA solution with fabricated membranes. As shown in Fig. 8, the permeate flux of the nanocomposite membranes is higher than the pure CA membrane. The enhanced permeate flux of nanocomposite membranes was significantly correlated to the enhanced hydrophilicity of the membrane surface. Furthermore, at a constant weight fraction of NPs, the flux of the CA/ND-PEG (0.5 wt.%) nanocomposite membrane is higher than the CA/ND (0.5 wt.%) nanocomposite membrane due to the inherent hydrophilicity of PEG that makes the CA membrane more permeable.

Protein rejection analysis

The protein rejection analyses of neat and nanocomposite membranes were investigated by measuring the concentration of BSA protein in

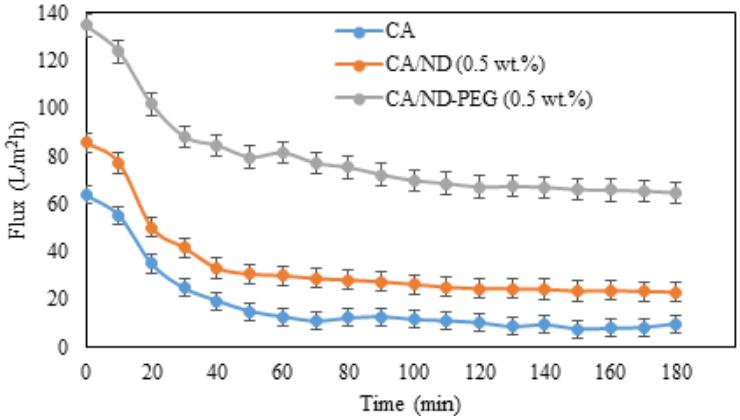

Fig. 8. Flux-time behavior of pure CA, CA/ND (0.5 wt.%), CA/ND-PEG (0.5 wt.%) membranes during filtration of 1 g/L BSA solution.

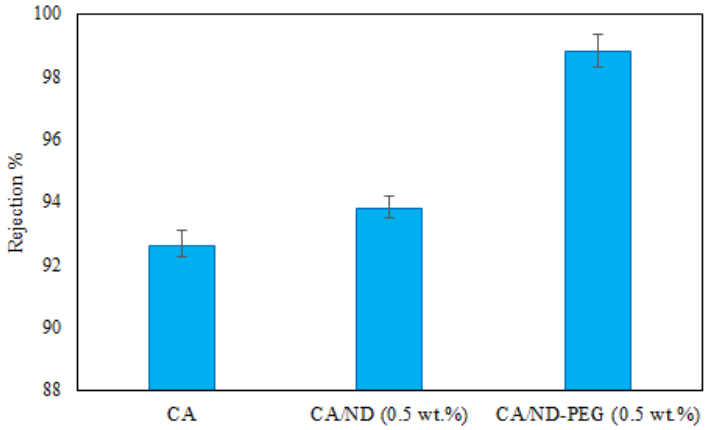

Fig. 9. Rejection performance of pure CA, CA/ND (0.5 wt.%), CA/ND-PEG (0.5 wt.%) membranes.

the feed and permeate streams using Eq. (12); the obtained results are summarized in Fig. 9.

As can be seen in Fig. 9, the BSA rejection increased from 92.6% to 93.8% by adding ND into the casting solution up to 0.5wt%. As mentioned earlier, the size of macrovoids decreased in the presence of neat ND particles than pure CA membrane; while the surface hydrophilicity of membranes increased due to the reduction of interaction between the BSA molecules and the membrane surface, which resulted in enhanced protein rejection. It can be seen that an increase in the protein rejection of ND-PEG embedded CA membrane is more pronounced than in pure ND embedded CA membrane. The presence of PEG in the CA/ND-PEG (0.5 wt.%) nanocomposite membrane prevents the adhesion of BSA inside the walls of pares due to steric stabilization effect of PEG which caused lower amounts of BSA particles can enter the membrane pores and consequently lower the amounts of BSA particles passing through the membrane while increasing the BSA rejection.

Fouling analysis

Hermia's model was applied to identify the fouling phenomenon occurring during the ultrafiltration processes. Prevailing fouling mechanism can be determined by fitting the experimental data into four models described earlier. The experimental data were substituted in the linearized equations of Hermia, shown in Table 1, and k values were determined as the slope of the line. Then, the k values were used to plot the flux equations and compared with experimental data. The obtained k values and correlation coefficient (R^2) are summarized in Table 4.

Figs. 10a-c compare the experimental data and fouling models for pure CA, CA/ND (0.5 wt.%) and CA/ND-PEG (0.5 wt.%) membranes, respectively.

As shown in these figures, it can be concluded that best fit to experimental data for all membranes corresponds to the cake layer formation model. This means that a layer of BSA is formed on the surface of membranes that impedes the entry of molecules into the membrane pore and keeps them back on the cake layer. It is interesting to note that cake filtration which occurred on the membrane surface, are types of reversible fouling that could be removed by physical cleaning methods.

The values of total fouling ratio (TFR), reversible

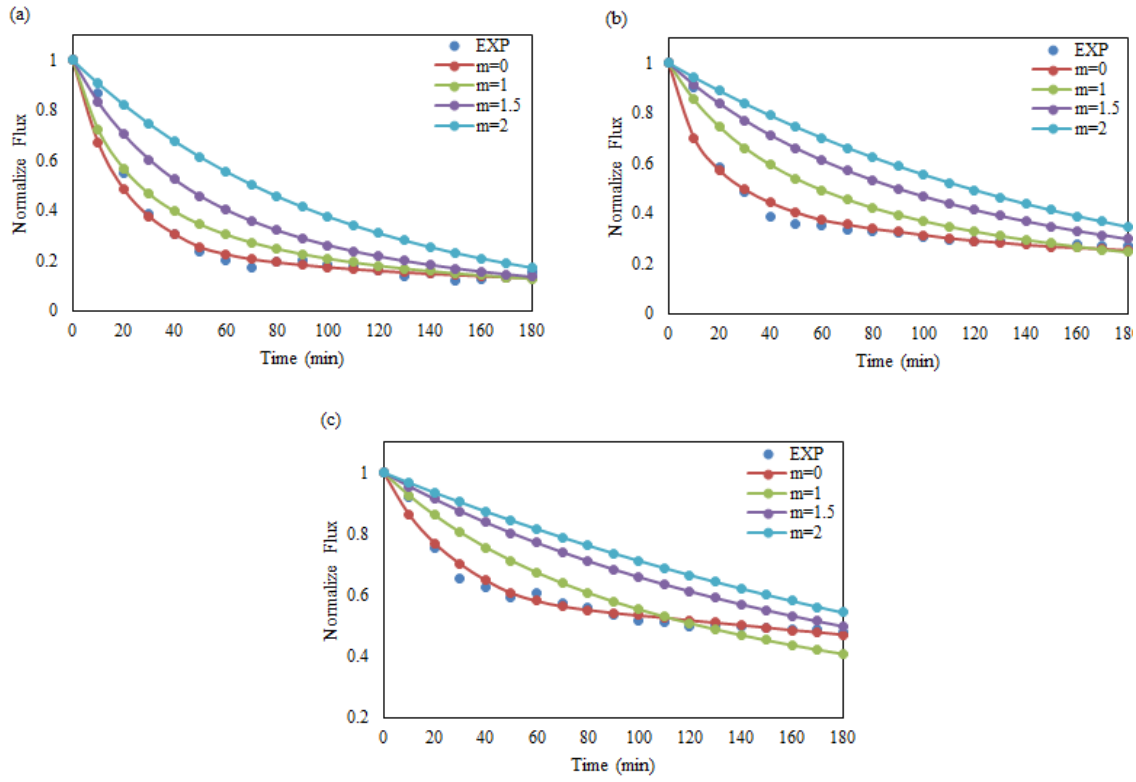

Fig. 10. Experimental data and Hermia fouling models for: (a) pure CA, (b) CA/ND (0.5 wt.%), (c) CA/ND-PEG (0.5 wt.%) membranes.

Table 4. Obtained k and correlation coefficient R^2 values for Hermia fouling models.

Membrane samples	m=0		m=1		m=1.5		m=2	
	k	R^2	k	R^2	k	R^2	k	R^2
Pure CA	8.00E-05	0.9606	6.00E-04	0.8728	1.20E-03	0.8337	9.80E-03	0.7625
CA/ND (0.5 wt.%)	1.00E-05	0.9388	2.00E-04	0.8295	5.00E-04	0.7715	5.90E-03	0.7066
CA/ND-PEG (0.5 wt.%)	1.00E-06	0.9547	6.00E-05	0.8496	2.00E-04	0.8158	3.40E-03	0.7786

Table 5. Fouling parameters of membranes during BSA filtration.

Membrane	RFR (%)	IFR (%)	TFR (%)	FR (%)
CA	68.8	17.9	86.7	82.1
CA/ND (0.5 wt.%)	59.5	13.1	72.6	86.8
CA/ND-PEG (0.5 wt.%)	46.6	4.8	51.4	95.2

fouling ratio (RFR), irreversible fouling ratio (IFR) and flux recovery (FR) of pure and nanocomposite membranes were obtained according to Eqs. (8)-(11) and the results are depicted in Table 5.

The lower TFR and higher FR values mean higher the antifouling property of the membranes and vice versa. As shown in Table 5, the total fouling ratio of the nanocomposite membranes was lower in comparison with that of pure CA membrane, which confirms nanocomposite membranes exhibit higher fouling resistant than the pure CA membranes. Membrane fouling consists of both reversible and irreversible fouling. Reversible fouling is attributed to the fouling agents which are loosely attached to the membrane and therefore can be easily removed by hydraulic washing. Irreversible fouling is attributed to the tightly bounded foulants to the membrane, which can only be removed by chemical cleaning. As can be seen in Table 5, incorporation of NPs decreased IFR from 17.9% for pure CA membrane to 13.1% and 4.8% for CA/ND (0.5 wt.%) and CA/ND-PEG (0.5 wt.%) nanocomposite membranes, respectively. It is also observed in Table 5 that the membrane fouling is dominated by the resistance caused by reversible fouling which can be easily removed by pure water cleaning. The improvement in the antifouling performance of the nanocomposite membranes is due to the fact that with the addition of inorganic particle to the CA membrane, the hydrophilicity of the CA membrane is enhanced (Table 2) to reduce the interactions of the BSA molecules on membrane surface due to the strongly bound water molecules, formed a water layer and obstruct the binding of protein molecules to the membrane surfaces [2]. These results conform reasonably to the FR values. FR which is the main criterion to evaluate the hydraulic cleaning efficiency and reflect the membrane antifouling property where higher FR value corresponds to the better antifouling property for the membrane. As shown in Table 5, the nanocomposite membrane containing CA/ND-PEG NPs exhibits the maximum FR value of 95.2%.

CONCLUSION

The obtained results in the present work showed that surface hydrophilicity still plays a significant role in providing protein repellent property, which is essential in anti-fouling behavior of prepared MF/UF membrane for protein separation and purification processes.

It is also proved that among several non-effective, expensive tedious conventional surface modification techniques to prepare hydrophilic membrane surface, the addition of a very little amount of NPs seems to be efficient. The functionalization of NPs however, is an essential step in preparing the well-distributed uniform hydrophilized surface.

In the present work, hydrophilized ND with PEG molecules showed the best performance but it is very important to avoid any NPs aggregation in membrane matrix because it seriously declines the membrane hydrophilicity, porosity, water uptake, protein repellency, and mechanical strength. Thus, it would be a very important point to determine the threshold amount of NPs content in the CA matrix. Regarding the anti-fouling behavior of prepared membranes, it was found that the CA/ND-PEG (0.5 wt.%) nanocomposite membrane exhibits higher flux recovery than other membranes.

CONFLICT OF INTEREST

The authors declare that there are no conflicts of interest regarding the publication of this manuscript.

REFERENCES

1. Zhu X, Loo H-E, Bai R. A novel membrane showing both hydrophilic and oleophobic surface properties and its non-fouling performances for potential water treatment applications. Journal of Membrane Science. 2013;436:47-56.
2. Arthanareeswaran G, Sriyamunadevi T, Raajenthiren M. Effect of silica particles on cellulose acetate blend ultrafiltration membranes: Part I. Separation and Purification Technology. 2008;64(1):38-47.
3. Abedini R, Mousavi SM, Aminzadeh R. A novel cellulose acetate (CA) membrane using TiO2 nanoparticles: Preparation, characterization and permeation study. Desalination. 2011;277(1-3):40-5.
4. Rabiee H, Shahabadi SMS, Mokhtare A, Rabiei H, Alvandifar N. Enhancement in permeation and antifouling properties of PVC ultrafiltration membranes with addition of hydrophilic surfactant additives: Tween-20 and Tween-80. Journal of Environmental Chemical Engineering. 2016;4(4):4050-61.
5. Saxena A, Tripathi BP, Kumar M, Shahi VK. Membrane-based techniques for the separation and purification of proteins: An overview. Advances in Colloid and Interface Science. 2009;145(1-2):1-22.
6. Damodar RA, You S-J, Chou H-H. Study the self cleaning, antibacterial and photocatalytic properties of TiO2 entrapped PVDF membranes. Journal of Hazardous Materials. 2009;172(2-3):1321-8.
7. Jayalakshmi A, Rajesh S, Mohan D. Fouling propensity and separation efficiency of epoxidated polyethersulfone incorporated cellulose acetate ultrafiltration membrane in the retention of proteins. Applied Surface Science. 2012;258(24):9770-81.
8. Peter-Varbanets M, Margot J, Traber J, Pronk W. Mechanisms of membrane fouling during ultra-low pressure ultrafiltration. Journal of Membrane Science. 2011;377(1-2):42-53.
9. Kang S, Asatekin A, Mayes A, Elimelech M. Protein antifouling mechanisms of PAN UF membranes incorporating PAN-g-PEO additive. Journal of Membrane Science. 2007;296(1-2):42-50.
10. Le-Clech P, Chen V, Fane TAG. Fouling in membrane bioreactors used in wastewater treatment. Journal of Membrane Science. 2006;284(1-2):17-53.
11. Zhang S, Qiu G, Ting YP, Chung T-S. Silver–PEGylated dendrimer nanocomposite coating for anti-fouling thin film composite membranes for water treatment. Colloids and Surfaces A: Physicochemical and Engineering Aspects. 2013;436:207-14.
12. Govardhan B, Chandrasekhar SS, Sridhar S. Purification of surface water using novel hollow fiber membranes prepared from polyetherimide/polyethersulfone blends. Journal of Environmental Chemical Engineering. 2017;5(1):1068-78.
13. Jafarzadeh Y, Yegani R, Sedaghat M. Preparation, characterization and fouling analysis of ZnO/polyethylene hybrid membranes for collagen separation. Chemical Engineering Research and Design. 2015;94:417-27.
14. Nguyen A, Zou L, Priest C. Evaluating the antifouling effects of silver nanoparticles regenerated by TiO2 on forward osmosis membrane. Journal of Membrane Science. 2014;454:264-71.
15. Etemadi H, Yegani R, Babaeipour V. Study on the reinforcing effect of nanodiamond particles on the mechanical, thermal and antibacterial properties of cellulose acetate membranes. Diamond and Related Materials. 2016;69:166-76.
16. Behboudi A, Jafarzadeh Y, Yegani R. Enhancement of antifouling and antibacterial properties of PVC hollow fiber ultrafiltration membranes using pristine and modified silver nanoparticles. Journal of Environmental Chemical Engineering. 2018;6(2):1764-73.
17. Sprick C, Chede S, Oyanedel-Craver V, Escobar IC. Bio-inspired immobilization of casein-coated silver nanoparticles on cellulose acetate membranes for biofouling control. Journal of Environmental Chemical Engineering. 2018;6(2):2480-91.
18. Khoshsang H, Ghaffarinejad A, Kazemi H, Jabarian S, Synthesis of Mesoporous Fe3O4 and Fe3O4/C Nanocomposite for Removal of Hazardous Dye from Aqueous Media, Journal of Water and Environmental Nanotechnology. 2018; 3(3): 191-206.
19. Mukherjee R, De S. Adsorptive removal of phenolic compounds using cellulose acetate phthalate–alumina nanoparticle mixed matrix membrane. Journal of Hazardous Materials. 2014;265:8-19.
20. Akbari A, Yegani R, Pourabbas B. Synthesis of high dispersible hydrophilic poly(ethylene glycol)/vinyl silane grafted silica nanoparticles to fabricate protein repellent polyethylene nanocomposite. European Polymer Journal. 2016;81:86-97.
21. Mulopo J. Bleach plant effluent treatment in anaerobic membrane bioreactor (AMBR) using carbon nanotube/polysulfone nanocomposite membranes. Journal of Environmental Chemical Engineering. 2017;5(5):4381-7.
22. Etemadi H, Yegani R, Babaeipour V. Performance evaluation and antifouling analyses of cellulose acetate/nanodiamond nanocomposite membranes in water treatment. Journal of Applied Polymer Science. 2017;134(21).
23. Zhu Y, Xu X, Wang B, Feng Z. Surface modification and dispersion of nanodiamond in clean oil. China Particuology. 2004;2(3):132-4.
24. Huang TS, Tzeng Y, Liu YK, Chen YC, Walker KR, Guntupalli R, et al. Immobilization of antibodies and bacterial binding on nanodiamond and carbon nanotubes for biosensor applications. Diamond and Related Materials. 2004;13(4-8):1098-102.
25. Krueger A. The structure and reactivity of nanoscale diamond. Journal of Materials Chemistry. 2008;18(13):1485.
26. Medina O, Nocua J, Mendoza F, Gómez-Moreno R, Ávalos J, Rodríguez C, et al. Bactericide and bacterial anti-adhesive properties of the nanocrystalline diamond surface. Diamond and Related Materials. 2012;22:77-81.
27. Wehling J, Dringen R, Zare RN, Maas M, Rezwan K. Bactericidal Activity of Partially Oxidized Nanodiamonds. ACS Nano. 2014;8(6):6475-83.
28. Mochalin VN, Shenderova O, Ho D, Gogotsi Y. The properties and applications of nanodiamonds. Nature Nanotechnology. 2011;7(1):11-23.
29. Burns NA, Naclerio MA, Khan SA, Shojaei A, Raghavan SR. Nanodiamond gels in nonpolar media: Colloidal and

rheological properties. Journal of Rheology. 2014;58(5):1599-614.
30. Holt KB. Diamond at the nanoscale: applications of diamond nanoparticles from cellular biomarkers to quantum computing. Philosophical Transactions of the Royal Society A: Mathematical, Physical and Engineering Sciences. 2007;365(1861):2845-61.
31. Li C-C, Huang C-L. Preparation of clear colloidal solutions of detonation nanodiamond in organic solvents. Colloids and Surfaces A: Physicochemical and Engineering Aspects. 2010;353(1):52-6.
32. Mykhaylyk OO, Solonin YM, Batchelder DN, Brydson R. Transformation of nanodiamond into carbon onions: A comparative study by high-resolution transmission electron microscopy, electron energy-loss spectroscopy, x-ray diffraction, small-angle x-ray scattering, and ultraviolet Raman spectroscopy. Journal of Applied Physics. 2005;97(7):074302.
33. Akbari A, Yegani R, Pourabbas B, Behboudi A. Fabrication and study of fouling characteristics of HDPE/PEG grafted silica nanoparticles composite membrane for filtration of Humic acid. Chemical Engineering Research and Design. 2016;109:282-96.
34. Nguyen T, Roddick F, Fan L. Biofouling of Water Treatment Membranes: A Review of the Underlying Causes, Monitoring Techniques and Control Measures. Membranes. 2012;2(4):804-40.
35. Fan X, Su Y, Zhao X, Li Y, Zhang R, Ma T, et al. Manipulating the segregation behavior of polyethylene glycol by hydrogen bonding interaction to endow ultrafiltration membranes with enhanced antifouling performance. Journal of Membrane Science. 2016;499:56-64.
36. Idris A, Mat Zain N, Noordin MY. Synthesis, characterization and performance of asymmetric polyethersulfone (PES) ultrafiltration membranes with polyethylene glycol of different molecular weights as additives. Desalination. 2007;207(1-3):324-39.
37. Akbari A, Yegani R, Pourabbas B. Synthesis of poly(ethylene glycol) (PEG) grafted silica nanoparticles with a minimum adhesion of proteins via one-pot one-step method. Colloids and Surfaces A: Physicochemical and Engineering Aspects. 2015;484:206-15.
38. Rad I, Khodayari K, Hadi Alijanvand S, Mobasheri H. Interaction of polyethylene glycol (PEG) with the membrane-binding domains following spinal cord injury (SCI): introduction of a mechanism for SCI repair. Journal of Drug Targeting. 2014;23(1):79-88.
39. Arthanareeswaran G, Thanikaivelan P. Fabrication of cellulose acetate–zirconia hybrid membranes for ultrafiltration applications: Performance, structure and fouling analysis. Separation and Purification Technology. 2010;74(2):230-5.
40. Ali M, Zafar M, Jamil T, Butt MTZ. Influence of glycol additives on the structure and performance of cellulose acetate/zinc oxide blend membranes. Desalination. 2011;270(1-3):98-104.
41. Karmakar S, Bhattacharjee S, De S. Experimental and modeling of fluoride removal using aluminum fumarate (AlFu) metal organic framework incorporated cellulose acetate phthalate mixed matrix membrane. Journal of Environmental Chemical Engineering. 2017;5(6):6087-97.
42. Zhang X, Wang S, Fu C, Feng L, Ji Y, Tao L, et al. PolyPEGylated nanodiamond for intracellular delivery of a chemotherapeutic drug. Polymer Chemistry. 2012;3(10):2716.
43. Wang D, Tong Y, Li Y, Tian Z, Cao R, Yang B. PEGylated nanodiamond for chemotherapeutic drug delivery. Diamond and Related Materials. 2013;36:26-34.
44. Dasgupta J, Chakraborty S, Sikder J, Kumar R, Pal D, Curcio S, et al. The effects of thermally stable titanium silicon oxide nanoparticles on structure and performance of cellulose acetate ultrafiltration membranes. Separation and Purification Technology. 2014;133:55-68.
45. Charfi A, Ben Amar N, Harmand J. Analysis of fouling mechanisms in anaerobic membrane bioreactors. Water Research. 2012;46(8):2637-50.
46. Etemadi H, Yegani R, Seyfollahi M. The effect of amino functionalized and polyethylene glycol grafted nanodiamond on anti-biofouling properties of cellulose acetate membrane in membrane bioreactor systems. Separation and Purification Technology. 2017;177:350-62.
47. Aris A, Shojaei A, Bagheri R. Cure Kinetics of Nanodiamond-Filled Epoxy Resin: Influence of Nanodiamond Surface Functionality. Industrial & Engineering Chemistry Research. 2015;54(36):8954-62.
48. Zhang G, Lu S, Zhang L, Meng Q, Shen C, Zhang J. Novel polysulfone hybrid ultrafiltration membrane prepared with TiO2-g-HEMA and its antifouling characteristics. Journal of Membrane Science. 2013;436:163-73.
49. Lee J, Chae H-R, Won YJ, Lee K, Lee C-H, Lee HH, et al. Graphene oxide nanoplatelets composite membrane with hydrophilic and antifouling properties for wastewater treatment. Journal of Membrane Science. 2013;448:223-30.
50. Yuliwati E, Ismail AF. Effect of additives concentration on the surface properties and performance of PVDF ultrafiltration membranes for refinery produced wastewater treatment. Desalination. 2011;273(1):226-34.
51. Vatanpour V, Madaeni SS, Moradian R, Zinadini S, Astinchap B. Novel antibifouling nanofiltration polyethersulfone membrane fabricated from embedding TiO2 coated multiwalled carbon nanotubes. Separation and Purification Technology. 2012;90:69-82.
52. Zinadini S, Zinatizadeh AA, Rahimi M, Vatanpour V, Zangeneh H. Preparation of a novel antifouling mixed matrix PES membrane by embedding graphene oxide nanoplates. Journal of Membrane Science. 2014;453:292-301.
53. Younas H, Fei Y, Shao J, He Y. Developing an antibacterial super-hydrophilic barrier between bacteria and membranes to mitigate the severe impacts of biofouling. Biofouling. 2016;32(9):1089-102.
54. Chen X, Su Y, Shen F, Wan Y. Antifouling ultrafiltration membranes made from PAN-b-PEG copolymers: Effect of copolymer composition and PEG chain length. Journal of Membrane Science. 2011;384(1-2):44-51.